Heliyon 10 (2024) e30626

Contents lists available at ScienceDirect

Heliyon

journal homepage: www.cell.com/heliyon

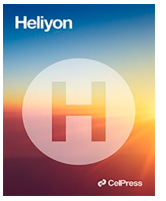

Research article

Analyzing the effects of polymeric dielectric materials on micro capacitive pressure sensors: A model incorporating displacement-dependent porosity

Nima Ahmadi [a], Ghader Rezazadeh [b,c,d,*], Arash Rahmani [e], Mina Ghanbari [f]

[a] Department of Mechanical Engineering, Technical and Vocational University (TVU), Tehran, Iran
[b] Center for Materials Technologies, Skolkovo Institute of Science and Technology, Moscow, Russia
[c] Mechanical Engineering Department, Urmia University, Urmia, Iran
[d] South Ural State University, Lenin Prospect 76, Chelyabinsk, 454080, Russia
[e] Renewable Energies Faculty, Mechanical Engineering Department, Urmia University of Technology, Urmia, Iran
[f] Mechanical Engineering Department, Engineering Faculty of Khoy, Urmia University of Technology, Urmia, Iran

ARTICLE INFO

Keywords:
Circular plate
Porous dielectric material
Displacement-dependent porosity
Frequency response
Nonlinear behavior
Learning approach

ABSTRACT

Recently, the extensive utilization of porous polymeric materials to amplify the sensitivity of capacitive devices is noticeable. The absence of an effective mathematical model for studying these devices has spurred the development of a comprehensive mathematical model in the current work. This model is formulated to analyze the static and dynamic behavior of systems incorporating a porous polymer dielectric material within the gap between flexible and fixed microplates. The derived nonlinear governing equations encompass the effects of electrostatic force, von-Karman nonlinear strains, and displacement-dependent porosity. Employing spatial decomposition, the resulting nonlinear algebraic equations and ordinary differential equations are leveraged to study the static and transient dynamic behavior, as well as the frequency response of the sensor using a learning approach. Two scenarios are investigated to assess the impact of various geometrical and physical parameters on sensor sensitivity one with a polymeric material and another without, each with distinct parameter values. The results reveal that the inclusion of a polymeric dielectric material increases electrostatic force but concurrently elevates the equivalent stiffness of the structure. The effectiveness of using a polymeric dielectric material is contingent upon the specific geometrical and physical properties of the sensor. Moreover, the obtained results in simplified cases are compared to existing numerical and experimental data, demonstrating a high degree of agreement. This work significantly contributes to advancing the understanding of sensors incorporating porous polymer dielectric materials and underscores their potential for enhanced sensitivity across diverse applications.

1. Introduction

Pressure values within various parts of the body, including the eye, brain cavity, kidney, bladder, blood vessels, and cerebrospinal fluid, serve as crucial indicators of a patient's health [1]. Continuous monitoring of pressure in these organs is vital for diagnosing

* Corresponding author. Center for Materials Technologies, Skolkovo Institute of Science and Technology, Moscow, Russia.
E-mail addresses: g.rezazadeh@skoltech.ru, g.rezazadeh@urmia.ac.ir (G. Rezazadeh).

https://doi.org/10.1016/j.heliyon.2024.e30626
Received 30 October 2023; Received in revised form 8 March 2024; Accepted 1 May 2024
Available online 3 May 2024

conditions and tracking disease progression [2,3]. In the realm of biomedical applications, micro-pressure sensors are gaining prominence for their ability to provide continuous pressure monitoring [4]. These sensors can be permanently placed on organs, transmitting signals to detect pressure variations.

Micro-pressure sensors come in various types, including piezoresistive pressure sensors [5,6], piezoelectric sensors [7], and capacitive pressure sensors [7–9]. Capacitive pressure sensors, in particular, stand out due to their straightforward design, accuracy, rapid response, repeatability, and low power consumption [10,11]. They find applications not only in biomedical settings but are also commonly used in electronic devices for industrial purposes, such as fingerprint detection.

Capacitive pressure sensors are designed with two elastic parallel plates serving as electrodes, separated by a Porous Polymer Dielectric Material. The capacitance of this capacitor is influenced by the material constant (ε), the electrode surface area (A), and the distance between them (d). Mechanical pressure applied to an electrode alters the distance between the plates and subsequently changes the capacitor's capacitance. This change in capacitance serves as an indication of pressure variation, allowing for pressure sensing [12].

In capacitive micro-pressure sensors, Porous Polymer Dielectric Materials are commonly utilized. The early use of these materials can be traced back to Wichterle and Lim's research, where a thin strip of Porous Polymer Dielectric Material was employed over a flexible substrate [13]. Additionally, Corkhill et al. utilized Porous Polymer Dielectric Materials in the development of contact lenses [14]. Peppas and Brannon, in 1991, proposed the use of these gels in hydrogel-based sensors [15]. Initially, hydrogels were employed as flexible medial layers for pressure sensing in capacitive sensors [16–18]. These hydrogels have evolved into three-dimensional structures, both in physical and chemical states, and have found applications in various fields, including drug delivery [19–21].

Advancements in micro and nanofabrication methods have led to the development of highly sensitive pressure sensors using hydrogels. Mannsfeld et al. designed pyramid-shaped, high-sensitivity, low-range microsensors [22]. Various studies have demonstrated that enhancing pressure sensor sensitivity can be achieved through the use of a porous elastomer as the dielectric layer or by injecting bubbles into the layer [23–25]. Beak et al. introduced a corrugated structure to reduce fabrication costs while increasing sensor sensitivity [26].

Polydimethylsiloxane (PDMS) was initially employed as the dielectric in a touch pressure sensor monitoring plantar pressure. However, its limited flexibility resulted in lower accuracy. Efforts have been made to enhance sensitivity by modifying the physical behavior of PDMS. Tee et al. fabricated sensors with various PDMS layer geometries to investigate their impact on microsensor sensitivity [27]. Li et al. designed a highly sensitive capacitive sensor using polystyrene as the dielectric and an innovative electrode pattern, although the process was complex and expensive [28].

Duan et al. used 3D printing to construct porous PDMS to achieve high sensitivity [29], but this method is considered expensive and complicated. Li et al. utilized the vacuum-assisted infiltration method to construct a more uniform porous PDMS, increasing construction speed and distributing the pores more uniformly [30]. Some studies focused on using sugar and other organic solvents for PDMS fabrication [31,32]. Xiao et al. fabricated a highly sensitive low-range pressure sensor using a porous polymer dielectric material for detecting human motion [33].

In recent years, numerous investigations have focused on enhancing the sensitivity of capacitive pressure sensors. Kang et al. [34] developed a mathematical and simulation model to increase sensor sensitivity by expanding the linear region beyond the conventional one. Xiao et al. [35] applied a composite dielectric to boost sensitivity by reducing Yang's modulus. They used Calcium Copper Titanate (CCTO) to fabricate a new membrane, introducing a certain level of porosity to enhance sensitivity [36,37]. Zhong et al. conducted research utilizing high-concentration carbon nanotubes as electrodes to achieve higher sensitivity, supported by a simple analytical model [38].

Guo et al. [39] fabricated an ultra-high sensitivity pressure sensor using a composite material prepared through the 3D printing method. Chauhan et al. [40] applied oxygen plasma treatment to create a Porous Polymer Dielectric Material without a limitation layer. This modification increased sensitivity and the maximum shear compared to sensors with a limitation layer. Achouch et al. [41] presented a novel design for a capacitive pressure sensor, modifying the distance between the diaphragm of the sensor to enhance its efficiency. They also proposed a new 3D printing method for sensor assembly.

As per the preceding content, there are references suggesting a viable mathematical model for a capacitive pressure sensor incorporating porous dielectric material. Consequently, this study aims to propose an innovative approach for effectively modeling the behavior of capacitive sensors. The research introduces a novel design of a capacitive pressure sensor featuring a polymer porous material as the dielectric within the flexible and fixed microplate gap. This design is then contrasted with the conventional model, which lacks a Porous Polymer Dielectric Material and relies on air within the gap. The research utilizes mathematical modeling to account for the nonlinearity of mid-plane stretching, electrostatic force, and displacement-dependent porosity. This approach is employed to investigate the static behavior, dynamic behavior, and Frequency Response of the models. The obtained results are compared with those of the conventional model. The expectation is that the sensitivity and performance of the innovative design are contingent upon the geometric and physical characteristics of the plates and polymer dielectrics.

2. Mathematical modeling

The 3D sight of the capacitive pressure sensor with flexible and fixed microplates which uses the porous polymer as a dielectric is presented in Fig. 1.

It should be noted that materials may behave differently at the micro- and sub-microscale, which must be taken into account in the model. Different length scales that affect observed interactions and phenomena have an impact on microscale behavior.

Several models exist to capture scale dependencies, including constitutive models such as the nonlocal Eringen model, higher-order

models such as couple stress theory, micropolar models, micromorphic models, and higher gradient models. It is important to note that obtaining the length scale properties required by many of these models can be challenging in experiments. Although length scale parameters have been reported for certain materials, designing appropriate experiments to obtain these length scales remains a challenge. When the length scale parameters approach the characteristic size of the structure, such as the thickness of a plate, the size dependence of the material becomes particularly apparent. It should be noted that the reported length scale for silicon is in the nanometer range [42,43].

However, given the nanoscale length scale of this study and the fact that the plate is made of silicon approximately one micron thick, it is unlikely that there is a significant size dependence in this particular situation. Therefore, in the current article, a classical model is used to model the bending of the plate. It should also be noted that for the porous elastomeric bed, as it experiences only a squeezing motion and bending does not take place, the use of couple stress theory or micropolar theory is not relevant to the problem.

The strains in the radial and peripheral directions which cause the circular plate transversal and radial displacements can be used using Föppl–von Kármán nonlinear strains in axisymmetric terms:

$$\varepsilon_r = \frac{\partial u}{\partial r} + \frac{1}{2}\left(\frac{\partial w}{\partial r}\right)^2 - z\frac{\partial^2 w}{\partial r^2} \tag{1}$$

$$\varepsilon_\theta = \frac{u}{r} - \frac{z}{r}\left(\frac{\partial w}{\partial r}\right) \tag{2}$$

where w and u are the lateral and radial movements of the plate in order. Therefore, r and z specify the radial and vertical situations in the circular plates.

The stress-strain correlation using Hook's theory can be achieved as follows:

$$\sigma_r = \frac{E}{1-\nu^2}\left\{\left[\frac{\partial u}{\partial r} + \frac{1}{2}\left(\frac{\partial w}{\partial r}\right)^2 + \nu\frac{u}{r}\right] - z\left(\frac{\partial^2 w}{\partial r^2} + \frac{\nu}{r}\left(\frac{\partial w}{\partial r}\right)\right)\right\} \tag{3}$$

$$\sigma_\theta = \frac{E}{1-\nu^2}\left\{\left[\nu\left(\frac{\partial u}{\partial r} + \frac{1}{2}\left(\frac{\partial w}{\partial r}\right)^2\right) + \frac{u}{r}\right] - z\left(\nu\frac{\partial^2 w}{\partial r^2} + \frac{1}{r}\left(\frac{\partial w}{\partial r}\right)\right)\right\} \tag{4}$$

So E, and ν denote Young's modulus and Poisson's ratio of the circular microplate. Regarding the radial and peripheral integration of stresses over microplate width radial and peripheral component of the force is extracted in the form of radial and lateral movements:

$$N_r = \frac{Eh}{1-\nu^2}\left[\frac{\partial u}{\partial r} + \frac{1}{2}\left(\frac{\partial w}{\partial r}\right)^2 + \nu\frac{u}{r}\right] \tag{5}$$

$$N_\theta = \frac{Eh}{1-\nu^2}\left[\nu\left[\frac{\partial u}{\partial r} + \frac{1}{2}\left(\frac{\partial w}{\partial r}\right)^2\right] + \frac{u_M}{r}\right] \tag{6}$$

In the last equation, h is the plate thickness, and referring to Newton's Second Law, the equation of radial and lateral displacement in the dynamic form by applying the electrostatic term of force is extracted as:

$$-\frac{1}{r}\left[\frac{\partial}{\partial r}(rN_r) - N_\theta\right] + \rho h\frac{\partial^2 u}{\partial t^2} + C_2\frac{\partial u}{\partial t} = 0 \tag{7}$$

$$\nabla^2\left(D\nabla^2 w\right) - \frac{1}{r}\left[\frac{\partial}{\partial r}\left(rN_r\frac{\partial w}{\partial r}\right)\right] + (\rho h)\frac{\partial^2 w}{\partial t^2} + C_1\frac{\partial w}{\partial t} + P_D - P_e - P(r,t) = 0 \tag{8}$$

where C_1 and C_2 are equivalent damping ratios, $D = \frac{Eh^3}{12(1-\nu^2)}$ is the bending rigidity of the membrane, P_D is a distributed pressure due to the compression of the porous dielectric material between two electrodes, $P(r,t)$ is the applied external pressure and P_e is the electrostatic term of the pressure due to the applied voltage to the flexible plate.

$$P_e = \frac{\kappa(p)\varepsilon_0 V^2}{2\left(h_f - \mathrm{w}\right)^2} \tag{9}$$

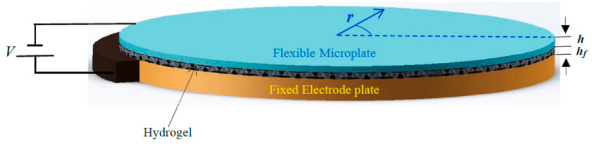

Fig. 1. The 3D model of the annular electrically actuated circular microplate using a porous polymer as the dielectric.

Where h_f represent the primary distance (gap) of the flexible and fixed microplates, ε_0 is the primitivity of the vacuum, and the applied voltage is indicated by V and shown in Fig. 1. κ is the dielectric coefficient of porous material filled between two electrodes. There are several models have been proposed for the dielectric coefficient of porous materials. Chong et al. [44] and Hou et al. [45] suggested an explicit relation for the dielectric of biphasic porous material. Also, several models have considered the main parameters of porosity like shape, size, configuration, and volume fraction [45]. While the dielectric of the porous materials is considered, some of these models can be interesting. For instance, Maxwell-Garnett takes into account the effects of the porosity of the polymer dielectric material and uses the volume fraction of voids [46]. The Brugman model is based on randomly distributed pores and calculates the dielectric constant according to the shape and volume fraction of pores [47]. Landau-Lifshitz-Looyenga (LLL) theory is the modified model of the Maxwell-Garnett which has included both the porosity and the shapes of pores. In this model, the shape of pores is assumed to be ellipsoidal or cylindrical which provides a more accurate estimation [48]. Another model is the Self-Consistence which uses numerical models to take into account the interaction of the solid matrix and pores [48]. The network model is one of the famous models that investigates the effects of connected porous matrices, where the pores form a network of interconnected pathways [49]. The abovementioned models are widely used to provide a more accurate dielectric characteristic in porous materials [45]. These models introduce a better viewpoint to investigate the impact of porosity on the dielectric behavior of porous materials [50]. Xing-Da Liu et al. have presented a general model to obtain the relative dielectric constant for through-hole as well as closed-pore materials as follows [51]

$$\kappa(p)=\kappa_s\frac{\left(\kappa_p+\gamma\kappa_s\right)+\forall_p\gamma\left(\kappa_p-\kappa_s\right)}{\left(\kappa_p+\gamma\kappa_s\right)-\forall_p\left(\kappa_p-\kappa_s\right)} \tag{10}$$

where (p) , κ_s and κ_p are the relative dielectric constant of the porous material, matrices material, and pore material respectively. $\forall_p$ is the volume fraction of the pore material, and γ is the structure factor 1 and 3 for through-hole and closed-pore materials, respectively. One of the most common cases is the case when the pore holes are through-hole or open-type holes. In this case, the structure parameter β is equal to 1.

The boundary condition is a critical factor influencing the behavior of the device. In the current scenario, where the flexible circular plate is assumed to be clamped along its edges, the boundary conditions can be outlined as follows

$$w(R,t)=0;\quad \left.\frac{\partial w(r,t)}{\partial r}\right|_{r=R}=0; \tag{11}$$

Since the out-plane or lateral stiffness of the circular plate is significantly reduced compared to the in-plane component, consequently, the natural frequencies of the lateral vibration modes are lower when compared with the in-plane modes. Consequently, the radial movement is surpassed by the lateral one to a significant extent. Consequently, the inertial forces of the radial displacement can be disregarded at lower frequencies. Thus, the nonlinear equation of the circular microplate with clamped edges, employing the averaging of the radial displacement force, can be derived as [52,53]:

$$\Re_1(w)=\nabla^2\left(D\nabla^2w\right)-\frac{Eh}{1-\upsilon^2}\left(\frac{1}{2R}\int_0^R\left(\frac{\partial w}{\partial r}\right)^2dr\right)\nabla^2w+(\rho h)\frac{\partial^2w}{\partial t^2}+c\frac{\partial w}{\partial t}+P_f-P_e-P(r,t)=0 \tag{12}$$

The Laplacian and bi-Laplacian operators are shown by ∇^2 and ∇^4 in order. If the axisymmetric condition is the ruler, the relations are:

$$\nabla^2=\frac{\partial^2}{\partial r^2}+\frac{1}{r}\frac{\partial}{\partial r},\ \nabla^4=\frac{\partial^4}{\partial r^4}+\frac{2}{r}\frac{\partial^3}{\partial r^3}-\frac{1}{r^2}\frac{\partial^2}{\partial r^2}+\frac{1}{r^3}\frac{\partial}{\partial r} \tag{13}$$

The mid-plane tension because of the clamped edges is demonstrated as the second term of equation (12). This term is due to the coupled in-plane and lateral displacement of the circular plate. So, it can be neglected in the small displacements and it should be significant in the large motions. It should be mentioned that it is averaged with the radius of the plate [54].

To simulate the influence of the polymeric porous dielectric material positioned between two electrodes, we take into account the squeezing motion of the polymeric material. As the polymeric material is porous, porosity typically results in a reduced Poisson's ratio [55]. Consequently, for this analysis, we assume a Poisson's ratio of zero, and we neglect strain in the radial direction, focusing solely on the strain in the axial (z) direction caused by its squeezing. Therefore, when considering the compression of the polymeric material as $w_f(r,z,t)$, the volume or bulk strain can be expressed as follows

$$\varepsilon_f^{(v)}=\frac{\partial w_f}{\partial z}+1 \tag{14}$$

Porous polymer deformation modeling involves developing mathematical and computational models to describe the mechanical behavior of hydrogels with interconnected pores or void spaces. Porous hydrogels are of particular interest in various applications, such as tissue production, drug delivery, and biomedical implants, due to their ability to accommodate fluid flow and provide a favorable environment for cell growth and tissue regeneration. In porous elastomers, two main models have explained the correlation between stress and strain (deformation), and the influences of the porosity have been included. Some of the subcategories of these models are:

The neo-Hookean model is simple and more accurate and has been used to model the stress and strain of elastomers which act like rubber materials [55]. In this model, the treatment is supposed to be completely elastic, and the stress is a function of the Green-Lagrange strain tensor. But, in this model, the effects of the porosity are not considered. The Ogden model which is widely used for porous rubber-like materials is a hyperelastic stress-strain model [55]. This model can calculate the strain-stiffening and strain-softening manner in elastomers. The Yeoh model [55] which considers the porosity effects is a nonlinear model which is used in elastomers with nonlinear stress-strain behavior. Gent model which is used in incompressible materials and relates the stretch to the exerted stress in the materials [56]. The stretch-strain model which calculates the rate of the strain in the elastomers is called the Arruda-Boyce model [56]. This model is modified to include the porosity effects in some applications. There is another model that combines the theories of stress-strain and stretch-stress considering the effects of porosity, which has been called the Poroviscoelastic model [56,57]. This model takes into account the fluid flow in the pores and the mechanical manner of the solid matrix. However, in the current case, since it is assumed that the volume changes in the porous polymeric material are primarily due to variations in pore volume, the volume fraction of porosity can be considered a function of the displacement of the polymeric material and can be expressed as follows

$$\forall_p = \begin{cases} \left(\forall_p^{(0)} + \frac{\partial w_f}{\partial z}\right)\left(1 + \frac{\partial w_f}{\partial z}\right)^{-1} & \forall_p^{(0)} + \frac{\partial w_f}{\partial z} > 0 \\ 0 & \forall_p^{(0)} + \frac{\partial w_f}{\partial z} \le 0 \end{cases} \tag{15}$$

Due to the earlier assumption of a Poisson's ratio of zero, the uniaxial squeezing or compressional motion of the polymeric porous material can be expressed using Newton's second law:

$$\frac{\partial \sigma}{\partial z} = \left(\rho_s \forall_s + \rho_p \forall_p\right) \frac{\partial^2 w_f}{\partial t^2} \tag{16}$$

In the above equation, ρ_s, and ρ_p are the density of the solid phase and fluid phase of the porous material respectively. Taking into account the relatively small deformation and adopting a strain-stress approach for the polymeric material, Equation (16) can be expressed as follows:

$$\frac{\partial}{\partial z}\left(E_f \frac{\partial w_f}{\partial z}\right) = \left(\rho_s \forall_s + \rho_p \forall_p\right) \frac{\partial^2 w_f}{\partial t^2} \tag{17}$$

Also, several proposed models vindicate the elastic modulus relation with the porosity in polymeric materials [58]. In these models, changing the porosity leads to a variation in the mechanical properties of the material. Some well-known models are listed below:

The Guth-Gold model [59] provides an experimental correlation in which Young's modulus is a function of the porosity of the material which is suggested by the $\frac{E}{E_0} = (1 - \forall_p)^3$. In this formula, E is Young's modulus of the porous material, E_0 is Young's modulus of the solid part, and $\forall_p$ is the porosity. There is a modified version of the Guth-Gold model whose name is the Lewis-Nielsen model [59]. In this model, the shape of the pores is ellipsoidal and it is given by $E = E_0(1 - \forall_p)^3(1 + k \bullet \forall_p)$. In the recent equation, k is the shape factor. The Voigt-Reuss-Hill Model consists of three parts: In the Voigt model the porous material is harder than the solid one. However, in the Reuss theory, the porous material is assumed to be softer. The Hill theory is the average of both mentioned theories [60]. Kerner's Model provided a micromechanical model that included the impact of the porosity and shape of the pores in Young's modulus [60]. Gibson-Ahby model accounts for the shape of the pores and relative density which is a cellular solids model [60,61]. There is another model which is an experimental theory that relates the relative density to Young's modulus and is called the Density-Stiffness Power Law model [60]. The mentioned models can estimate the mechanical properties of porous materials like polymers and elastomers etc. The accuracy of these models is highly dependent on the material mechanical properties and pore size. Therefore, experimental verification is inevitable [51].

$$E_f = E_s\left(1 - \frac{\forall_p}{\forall_p^{(c)}}\right) \tag{18}$$

Combination of equations (17) and (18) results:

$$\frac{\partial}{\partial z}\left[\left(E_s\left(1 - \frac{\forall_p}{\forall_p^{(c)}}\right)\right)\frac{\partial w_f}{\partial z}\right] = \left(\rho_s \forall_s + \rho_p \forall_p\right) \frac{\partial^2 w_f}{\partial t^2} \tag{19}$$

Therefore, equation (19) can be rearranged as follows:

$$\frac{\partial}{\partial z}\left[\left(E_s \frac{1}{\forall_p^{(c)}}\left(\forall_p^{(c)} - \left(\forall_p^{(0)} + \frac{\partial w_f}{\partial z}\right)\left(1 + \frac{\partial w_f}{\partial z}\right)^{-1}\right)\right)\frac{\partial w_f}{\partial z}\right] = \left(\rho_s \forall_s + \rho_p\left(\forall_p^{(0)} + \frac{\partial w_f}{\partial z}\right)\left(1 + \frac{\partial u_f}{\partial z}\right)^{-1}\right)\frac{\partial^2 w_f}{\partial t^2} \tag{20}$$

For the small displacements (Below 10 %), for convenience, the non-linear term can be approximated by Taylor expansion as follows:

$$\left(1+\frac{\partial w_f}{\partial z}\right)^{-1} \approx 1-\frac{\partial w_f}{\partial z} \tag{21}$$

Hence, substituting relation 21 in 20 eventuate:

$$\frac{\partial}{\partial z}\left[\left(E_s\frac{1}{\forall_p^{(c)}}\left(\forall_p^{(c)}-\left(\forall_p^{(0)}+\frac{\partial w_f}{\partial z}\right)\left(1-\frac{\partial w_f}{\partial z}\right)\right)\right)\frac{\partial w_f}{\partial z}\right]=\left(\rho_s\forall_s+\rho_p\left(\forall_p^{(0)}+\frac{\partial w_f}{\partial z}\right)\left(1-\frac{\partial w_f}{\partial z}\right)\right)\frac{\partial^2 w_f}{\partial t^2} \tag{22}$$

Re-arranging equation (22) suggests the newest form of the equation,

$$\frac{E_s}{\forall_p^{(c)}}\frac{\partial}{\partial z}\left[\left(\forall_p^{(c)}-\forall_p^{(0)}-\frac{\partial w_f}{\partial z}+\forall_p^{(0)}\frac{\partial w_f}{\partial z}+\left(\frac{\partial w_f}{\partial z}\right)^2\right)\frac{\partial w_f}{\partial z}\right]=\left(\rho_s\forall_s+\rho_p\left(\forall_p^{(0)}+\frac{\partial w_f}{\partial z}-\forall_p^{(0)}\frac{\partial w_f}{\partial z}-\left(\frac{\partial w_f}{\partial z}\right)^2\right)\right)\frac{\partial^2 w_f}{\partial t^2} \tag{23}$$

For weak formulation by using the finite element method, equation (23) can be presented as:

$$\begin{aligned}\Re_2(w_f)=&\frac{E_s}{\forall_p^{(c)}}\left[\left(\forall_p^{(c)}-\forall_p^{(0)}-\frac{\partial w_f}{\partial z}+\forall_p^{(0)}\frac{\partial w_f}{\partial z}+\left(\frac{\partial w_f}{\partial z}\right)^2\right)\frac{\partial^2 w_f}{\partial z^2}\right]+\frac{E_f^{(0)}}{\forall_p^{(c)}}\left[\left(-\frac{\partial^2 w_f}{\partial z^2}+\forall_p^{(0)}\frac{\partial^2 w_f}{\partial z^2}+2\frac{\partial^2 w_f}{\partial z^2}\left(\frac{\partial w_f}{\partial z}\right)\right)\frac{\partial w_f}{\partial z}\right]-\rho_s\forall_s\frac{\partial^2 w_f}{\partial t^2}\\&-\rho_p\left(\forall_p^{(0)}+\frac{\partial w_f}{\partial z}-\forall_p^{(0)}\frac{\partial w_f}{\partial z}-\left(\frac{\partial w_f}{\partial z}\right)^2\right)\frac{\partial^2 w_f}{\partial t^2}=0\end{aligned} \tag{24}$$

The foundation force term and boundary conditions for the solution of equation (24) are presented as follows:

$$P_f(r,0,t)=\left(E_f\frac{\partial w_f}{\partial z}\right)\Big|_{z=0}, w_f(r,0,t)=\mathrm{w}(r,t), w_f(r,h_f,t)=0, \tag{25}$$

In the current context, it's important to note that the upper boundary for the polymeric dielectric material is moving. However, when the plate deflection is significantly smaller than the height of the dielectric material, it can be overlooked, although it remains a time-varying boundary.

2.1. Numerical solution

Obtaining an analytical solution that strongly satisfies the governing equation throughout the entire domain is often challenging. Consequently, one of the prevalent methods involves meeting the governing equation in its weak form through various integral representations. One notable approach is the Galerkin weighted residual method, which is equivalent to the principle of virtual work [52,62]. In this approach, the infinite solution space is substituted with a finite one where convergence is guaranteed. The solution is then decomposed using the basis functions of the solution space. The basis function should satisfy the accompanying boundary conditions. Given that the boundary condition for the squeezing motion of the dielectric material is time-varying, decomposing the solution into the following form results in a homogeneous Dirichlet boundary condition for u.

$$w_f=u+\left(1-\frac{z}{h_f}\right)w \tag{26}$$

At the interface of the circular plate and the hydrogel, the displacement of the plate and the hydrogel are the same, so:

$$u(r,0,t)=0 \tag{27}$$

On the other side, the displacement of the hydrogel is limited to the fixed plate, hence:

$$u(r,h_f,t)=0 \tag{28}$$

To address equations 12 and 24 through a spatial decomposition method, it is assumed that the transverse motion of the plate and the squeezing motion of the polymeric material can be expressed as the product of established spatial shape functions ($\varphi_n(r)$, $\psi_m(z)$). These functions adhere to the boundary conditions and are applied to unknown time-dependent functions ($a_n(t)$ and $b_{nm}(t)$) in a series form [61]:

$$w(r,t)=\sum_{n=1}^{\infty}a_n(t)\varphi_n(r) \tag{29}$$

$$u(r,z,t)=\sum_{n=1}^{\infty}\sum_{m=1}^{\infty}b_{nm}(t)\varphi_n(r)\psi_m(z) \tag{30}$$

Taking into account that the pivotal contributions come from the initial terms, the infinite series can be truncated to a finite series. This results in a reduction of the solution space dimension to a finite one. It's important to note that the convergence of this truncated series needs to be verified.

$$w^N(r,t)=\sum_{n=1}^{N}a_n(t)\varphi_n(r) \tag{31}$$

$$u^{NM}(r,z,t)=\sum_{n=1}^{N}\sum_{m=1}^{M}b_{nm}(t)\varphi_n(r)\psi_m(z) \tag{32}$$

The introduction of reduced-order model solutions through substitution results in the following errors.

$$\Re_1\left(u^{NM},w^N\right)=\mathfrak{E}_1 \tag{33}$$

$$\Re_2\left(u^{NM},w^N\right)=\mathfrak{E}_2 \tag{34}$$

Alternatively, in expanded form, the errors can be expressed as follows.

$$\Re_1\left(u^{NM},w^N\right)=D\sum_{n=1}^{N}r^3a_n(t)\varphi_n^{(4)}(r)+2D\sum_{n=1}^{N}r^2a_n(t)\varphi_n^{'''}(r)-D\sum_{n=1}^{N}ra_n(t)\varphi_n^{''}(r)+D\sum_{n=1}^{N}a_n(t)\varphi_n^{'}(r)+\frac{Eh}{2R(1-\nu^2)}\sum_{m=1}^{N}\sum_{s=1}^{N}\times\sum_{n=1}^{N}\left\{a_ma_sa_n\left(\varphi_n^{''}(r)+\frac{1}{r}\varphi_n^{'}(r)\right)\right\}\int_0^R\left(\varphi_s^{'}(r)\varphi_m^{'}(r)\right)dr+\rho h\sum_{n=1}^{N}\ddot{a}_n(t)\varphi_n(r)+c\sum_{n=1}^{N}\dot{a}_n(t)\varphi_n(r)-P_e(r,t)+P_f(r,t)+P(r,t)=\mathfrak{E}_1 \tag{35}$$

$$\Re_2\left(u^{NM},w^N\right)=\frac{E_f^{(0)}}{\forall_p^{(c)}}\left(\left(2\forall_p^{(0)}-2\right)\sum_{n=1}^{N}\sum_{m=1}^{M}b_{nm}^2\varphi_n^2\psi_m^{'}\psi_m^{''}+\frac{\left(2-2\forall_p^{(0)}\right)}{h_f}\sum_{n=1}^{N}\sum_{m=1}^{M}a_nb_{nm}\varphi_n^2\psi_m^{''}+3\sum_{n=1}^{N}\sum_{m=1}^{M}b_{nm}^3\varphi_n^3\psi^{'2}{}_m\psi_m^{''}-\frac{6}{h_f}\sum_{n=1}^{N}\times\sum_{m=1}^{M}a_nb_{nm}^2\varphi_n^3\psi_m^{'}\psi_m^{''}+\frac{3}{h_f{}^2}\sum_{n=1}^{N}\sum_{m=1}^{M}a_n{}^2b_{nm}\varphi_n{}^3\psi^{''}{}_m\right)-\rho_s\forall_s\sum_{n=1}^{N}\sum_{m=1}^{M}\ddot{b}_{nm}\varphi_n\psi_m-\rho_s\forall_s\sum_{n=1}^{N}\ddot{a}_n\varphi_n+\frac{\rho_s\forall_s}{h_f}z\sum_{n=1}^{N}\ddot{a}_n\varphi_n=\mathfrak{E}_2 \tag{36}$$

Given that the provided solutions do not satisfy the governing equations in a strong form, an expectation arises for a weak integral form of satisfaction. Consequently, a weighted integral of the errors is compelled to be zero [52,63]. This imposition serves to balance the system from an energy perspective.

$$\int_0^R\Re_1\left(u^{NM},w^N\right)\varphi_j(r)dr=0,j=1,\ldots,N \tag{37}$$

$$\int_0^{h_f}\int_0^R\Re_2\left(u^{NM},w^N\right)\varphi_i(r)\psi_j(z)drdz=0,i=1,\ldots,N,j=1,\ldots,M \tag{38}$$

Balancing the energy of the system yields a set of $N+N\times M$ time-dependent ordinary differential equations (ODEs). By solving these equations, the unknowns can be determined as functions of time.

In a static analysis, it's crucial to note that the time-dependent unknowns simplify to algebraic parameters because the inertial terms become zero. In the dynamic case, where the transient response of the system is required, achieving it involves direct integration over time. Integration methods such as the fourth-order Runge-Kutta method can be employed for this purpose.

The transient response provides crucial insights into the system's behavior during initial stages or under changing conditions, offering a comprehensive view of its dynamics. It illuminates how the system evolves, capturing nuances in its response to sudden changes or external stimuli. On the other hand, the frequency response is indispensable for analyzing how the system reacts to various input frequencies. It helps uncover details about the system's stability, resonance characteristics, and overall performance under different frequency conditions.

Therefore, a comprehensive analysis of dynamic systems demands both a thorough exploration of transient response, which reveals the system's time-dependent behavior, and a meticulous examination of frequency response, which unveils its frequency-dependent characteristics. Together, these analyses provide a holistic understanding of the system's dynamic behavior across different time scales and frequency domains.

In linear systems, finding the frequency response is relatively straightforward. However, when dealing with nonlinear systems, the presence of nonlinear terms introduces complexity. Depending on the order of these nonlinear terms, various methods are suggested for analysis. These methods include harmonic balance, averaging, time scaling, and numerical shooting methods. Each approach addresses specific challenges posed by nonlinearities, offering effective ways to analyze and understand the system's behavior under different conditions. However, all of the aforementioned methods come with inherent limitations and complexities, especially when dealing with a system of nonlinear equations.

In this context, the steady-state solution of the nonlinear system is presented in an N-dimensional Fourier series, and the unknown coefficients are then determined by balancing the energy of the system in a period through a learning approach. This alternative method aims to overcome the challenges associated with the traditional techniques, offering a potentially more effective and robust way to analyze and solve complex nonlinear systems [24,25].

To find the unknown coefficients of the series, we begin with initial values derived from the linear solution and iteratively update

them using a physically based learning method. The aim is to guarantee that, within a given time frame, the updated coefficients fulfill the governing equations from an energy viewpoint. This method has the advantage of effectively determining the amplitudes of higher harmonics. Moreover, this method permits sweeping frequencies within a range, facilitating the investigation of primary and secondary resonances across all harmonics. Nevertheless, it presents a significant drawback in the form of identifying and refining unstable solutions, which remains a complex technical challenge. Although the method has its drawbacks, it remains valuable for its comprehensive analysis and ability to capture complex nonlinear dynamics. This is particularly the case in scenarios featuring higher harmonics and varied frequency sweeps. However, to implement this method in the current study, the unidentified coefficients $a_n(t)$, and $b_{nm}(t)$ can be represented as an (N + M)-dimensional vector.

$$\overrightarrow{\mathbb{Q}}(\widehat{t}) = \{\ a_1\ a_2\ a_3 \ldots a_N\ \ b_{11}\ b_{12}\ b_{13} \ldots b_{1N}\ \ldots\ b_{M1}\ b_{M2}\ b_{M3} \ldots b_{MN}\ \}^T \tag{39}$$

Equations (37) and (38) can be amalgamated and expressed as:

$$\Re\left(\overrightarrow{\mathbb{Q}}(\widehat{t})\right) = 0 \tag{40}$$

To examine the frequency response of the system of nonlinear coupled equations, the solution to Equation (40) can be expressed as a series of sine and cosine functions.

$$\overrightarrow{\mathbb{Q}}^{(i)}(\widehat{t}) = \left\{\Phi_0^{(i)} + \sum_{j=1}^{S}\left(\Phi_j^{(i)}\ cos(j\Omega\widehat{t}) + \Psi_j^{(i)}\ sin(j\Omega\widehat{t})\right)\right\}, i = 1, \ldots, (N+M)\ \mathrm{A}_j^{(i)} = \sqrt{\left(\Phi_j^{(i)}\right)^2 + \left(\Psi_j^{(i)}\right)^2} \tag{41}$$

Here, $\mathrm{A}_j^{(i)}$ represents the dimensionless amplitude of the frequency response at the $\mathrm{j_{th}}$ harmonic. Substitution Eq. (41) into Eqs. (37) and (38) leads to the errors as:

$$\Re\left(\overrightarrow{\mathbb{Q}}^{(i)}(\widehat{t})\right) = \varepsilon^{(i)}(\widehat{t}), i = 1, \ldots, (N+M) \tag{42}$$

If a system of ordinary nonlinear equations in the time domain displays periodic behavior, it may be reformulated as a boundary value problem. Consequently, the starting and ending points of the period serve as boundaries, and the solution can be obtained via a weak formulation, often expressed using an integral representation. One of the most common weak formulations involves implementing the Galerkin weighted residual method, which is fundamentally equivalent to the principles of virtual work or the energy balance method. To establish the unknown coefficients, a trial-and-error approach is utilized and an initial value for the unknown coefficient is typically attained from a linear solution. Following the Jacobian definition, a learning approach is utilized to calculate the next set of trial coefficients via a Gradient Descent-based method. This provides insights into determining the unknown coefficients in subsequent steps.

In implementing a weak integrally satisfying method, the weighted residual or energy or cost function, denoted as $\overrightarrow{\Lambda}^{(i)}$, can be expressed at a given initial value for the coefficients as follows:

$$\overrightarrow{\Lambda}^{(i)} = \int_0^{\tau} \varepsilon^{(i)}(\widehat{t})\,\overrightarrow{w}_k(\widehat{t})\,d\widehat{t}, k = 0, 1, 2, 3, \ldots 2s \tag{43}$$

where τ is the integration limit and can be the period of the response when the solution is a steady-state, and $\overrightarrow{w}_k(\tau)$ is the weight function, which can be defined as:

$$\tau = (2\pi / \Omega)\ \overrightarrow{w}_k(\widehat{t}) = \{1, sin(k\Omega\widehat{t}), \cos(k\Omega\widehat{t})\}, k = 1, 2, 3, \ldots, s \tag{44}$$

The vector of unknown coefficients can be defined as:

$$\overrightarrow{Y}^{(i)} = \left\{\Phi_0^{(i)}, \Phi_1^{(i)} \ldots \Phi_s^{(i)}, \Psi_1^{(i)} \ldots \Psi_s^{(i)}\right\}^T \tag{45}$$

The value of the cost or energy function will be a function of unknown coefficients as:

$$\overrightarrow{\Lambda}^{(i)} = \widehat{F}\left(\overrightarrow{Y}^{(i)}\right) \tag{46}$$

From the Taylor expansion series, one can compute the energy or cost function value in terms of the variation of coefficients:

$$\overrightarrow{\Lambda}_{n+1}^{(i)} = \Lambda_n^{(i)} + \left[\frac{\partial\overrightarrow{\Lambda}^{(i)}}{\partial\overrightarrow{Y}^{(i)}}\Big|_{\overrightarrow{Y}^{(i)} = \overrightarrow{Y}_n^{(i)}}\right]\Delta\overrightarrow{Y}^{(i)} + O\left(\Delta\overrightarrow{Y}^{(i)}\right)^2 \tag{47}$$

Given that the desired value of the cost function is zero ($\overrightarrow{\Lambda}_{n+1}^{(i)} = 0$), the values of the unknown coefficients can be determined as:

$$\overrightarrow{Y}_{n+1}^{(i)} = \overrightarrow{Y}_n^{(i)} - \left[\frac{\partial\Lambda_n^{(i)}}{\partial\overrightarrow{Y}^{(i)}}\Big|_{\overrightarrow{Y}^{(i)} = \overrightarrow{Y}_n^{(i)}}\right]^{-1}\Lambda_n^{(i)} \tag{48}$$

It is noteworthy that the coefficients' initial values can be obtained from the linear solution. Following Eq. (48), this procedure will be repeated until attaining more precise outcomes, indicating the iteration's importance.

When dealing with a pressure sensor, the typical scenario involves subjecting the sensor to a biased DC voltage along with a static pressure that may fluctuate around its nominal value. However, in the context of CMUT (Capacitive Micromachined Ultrasonic Transducer) devices, where the objective is to generate harmonic pressure, the device can function as an actuator rather than a sensor. In this case, the system is exposed to both a bias DC voltage and an AC voltage. Therefore, to comprehensively address and generalize the findings in the article, both cases are thoroughly studied, and the inputs are considered in the following manner. This approach ensures a comprehensive exploration of the device's behavior under various operating conditions.

$$\mathrm{V} = V_{DC} + V_{AC}\sin(\omega t) \tag{49}$$

$$\mathrm{P} = P_0 + P_d \sin(\omega t) \tag{50}$$

2.2. Model validation

To validate the model, a circular micro-plate with a polymer porous case, which has not been considered before, is developed. To examine the method and verify the results of the present work, a common type of circular plate without the hydrogel is also studied. The extracted results (Fig. 2) for this case are compared to experimental results from Refs. [64,65] and numerical results from Ref. [66]. The validation process demonstrates a good agreement with the referenced results (see Table 1). It is important to note that the geometrical configurations and physical properties of the case study are deliberately chosen to match those outlined in the published works for a comprehensive and rigorous validation.

Fig. 2 shows the static pull-in voltage for the case without Porous Polymer Dielectric Material between the flexible and fixed micro-plates.

3. Results and discussion

The Galerkin weighted model is used in this study to create a reduced order model (ROM) through the decomposition of governing equations over spatial coordinates. The shape functions utilized in this procedure are provided below, satisfying all boundary conditions [67]. The reduced order model (ROM) is an effective approach for high-dimensional systems, offering greater computational efficiency for large-scale simulations. However, it is limited by complex geometries. The choice between a ROM approach using Hilbert space basis functions expansion and the Finite Element Method depends on the specific characteristics of the problem, including the system's dimensionality, computational efficiency requirements, and the need for high-fidelity solutions.

To examine the impact of employing Porous Polymer Dielectric Material in the gap between fixed and flexible plates, two cases with distinct states are considered. Case 1 and Case 2 involve circular plate diameters of 500 μm and 250 μm, respectively. Each case comprises two states: State 1 with air in the gap, and State 2 with Porous Polymer Dielectric material in the gap.

$$\varphi_n(r) = 1 + \cos\left(\frac{(2n-1)\pi \bullet r}{R}\right) \tag{51}$$

$$\psi_n(z) = \sin\left(\frac{n\pi z}{h_f}\right) \tag{52}$$

The geometrical and physical properties of cases 1 and 2 with states 1 and 2 which are studied in the present work are given in Table 2.

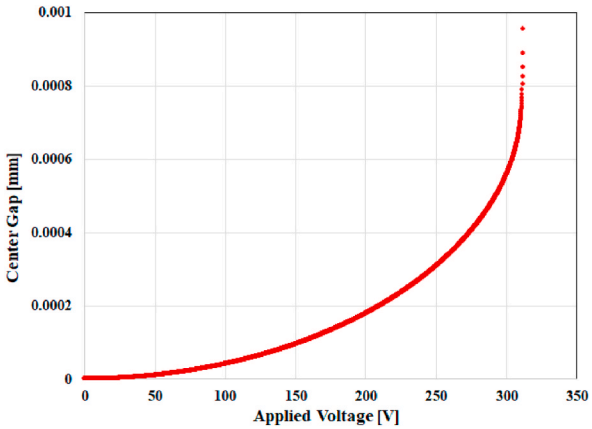

Fig. 2. Pull-in voltage for the case without Porous Polymer Dielectric Material.

Table 1
Comparison of the results to the results of published works [64–66].

Different cases in the numerical procedure	Pull-in Voltage of each voltage increment step			
	0.1	0.05	0.01	0.001
Results of the static pull-in voltages for N=3	312.8	312.65	312.56	312.421
Results of the static pull-in voltages for N=5	313.25	313.05	312.95	312.893
Results of the static pull-in voltages for N=10	313.25	313.05	312.95	312.891
Results of the static pull-in voltages for N=20	313.25	313.05	312.95	312.889
Comparison of the obtained results with available data	**%**			
Comparison of the results with [50]: (311.6 V)	0.53 %	0.46 %	0.43 %	0.41 %
Comparison of the results with [51]:(314V)	0.24 %	0.3 %	0.33 %	0.35 %

Table 2
Geometrical and physical properties of the case study [64,68,69].

Parameter	Symbol	Value
The radius of case 1	R	500 μm
The radius of case 2	R	250 μm
Circular microplate thickness (cases 1 and 2)	h	1 μm
Porous Polymer Dielectric Material thickness case 1	h_f	1 μm
Porous Polymer Dielectric Material thickness case 2	h_f	3 μm
Circular plate Young's Modulus	E	169 GPa
Poison's ratio of case 1	ν	0.43
Poison's ratio of case 2	ν	0.3
Circular plate density	ρ	2330 kg/m^3
Porous Polymer material Young's Modulus (case 1)	E_s	360 kPa
Porous zone fluid Young's Modulus (case 1)	$E_f^{(0)}$	288 kPa
Porous Polymer material Young's Modulus (case 2)	E_s	9.7 kPa
Porous zone fluid Young's Modulus (case 2)	$E_f^{(0)}$	7.6 kPa
Porous Polymer Dielectric Material density	ρ_s	965 kg/m^3
Porous zone fluid density	ρ_p	1.2 kg/m^3
The porosity of the polymer	$\forall_p^{(0)}$	0.1
Critical Porosity of polymer	$\forall_p^{(c)}$	0.5
Permittivity of air	ε_0	$8.8541878 \times 10^{-12}$ F/m

3.1. Static analysis

The results are obtained for both cases, with and without the Porous Polymer Dielectric Material, and a comparative analysis is performed. In the static analysis, equations are derived by eliminating time-independent terms in equations 37 and 38. Essentially, this involves assuming that the time-dependent derivatives are zero, and other time-dependent coefficients such as ($a_n(t)$ and $b_{nm}(t)$) are considered as constant, unknown coefficients. This assumption leads to a set of algebraic equations. To mitigate the impact of solution procedure errors, the applied voltage is gradually increased. Once the solution converges, the unknown coefficients (a and b) are determined. Subsequently, the displacement can be calculated using equations 31 and 32. It's worth noting that the displacement of the Porous Polymer Dielectric Material and the circular plate at the interface are equal. The pull-in voltage is crucial for limiting the device's applicable bias voltage range and defining its stable operational limits. This phenomenon occurs during a saddle-node bifurcation in the flexible plate. Accurately determining the pull-in voltage is essential for a comprehensive understanding of the system's behavior, guiding the device's stable operation and highlighting potential limitations under various conditions.

Fig. 3a–e, indicate the pull-in voltage and the displacement of the center of the circular microplate for cases 1 and 2. It is worth noting that, to increase confidence, the results of case 1 state 1 were simulated using COMSOL Multiphysics 6.1 as a three-dimensional model and compared with the current model, resulting in a good agreement. Fig. 3b displays the 3D contour of the central deflection upon application of voltage.

As it is clear, the Porous Polymer Dielectric Material causes different behavior in the system which depends on the system's geometrical and physical parameters. In case 1 state 2 it leads to the hardening of the system and it leads to a higher pull-in voltage compared with case 1 state 1. The pull-in voltage for state 1 is about 0.81V which is small enough from the 22V for state 2. Unlike in case 2, this phenomenon is vice versa. In case 2 state 1 the pull-in voltage is increased to 23.8V however, state 2 has a 9.8V pull-in voltage. It is obvious that in case 2, the Porous Polymer increased the sensitivity of the sensor. After achieving the pull-in voltage for each case, it is tried to model the effect of the bias voltage as a coefficient of the pull-in voltage plus a constant pressure. In other words, the constant pressure is applied and increased from 0 and the maximum value is achieved before the pull-in. The constant pressure is gradually increased from zero while the voltage is applied as a coefficient (β) of the pull-in voltage ($\beta = 0.3$, $\beta = 0.5$, and $\beta = 0.7$). Fig. 4a–d demonstrate the center displacement of the microplate while applying the constant pressure in a bias voltage. According to Fig. 4, it can be found that the maximum applied pressure is decreased while increasing the bias voltage for both cases. This is because by increasing the bias voltage, the displacement of the center is increased and the maximum pressure which can be applied

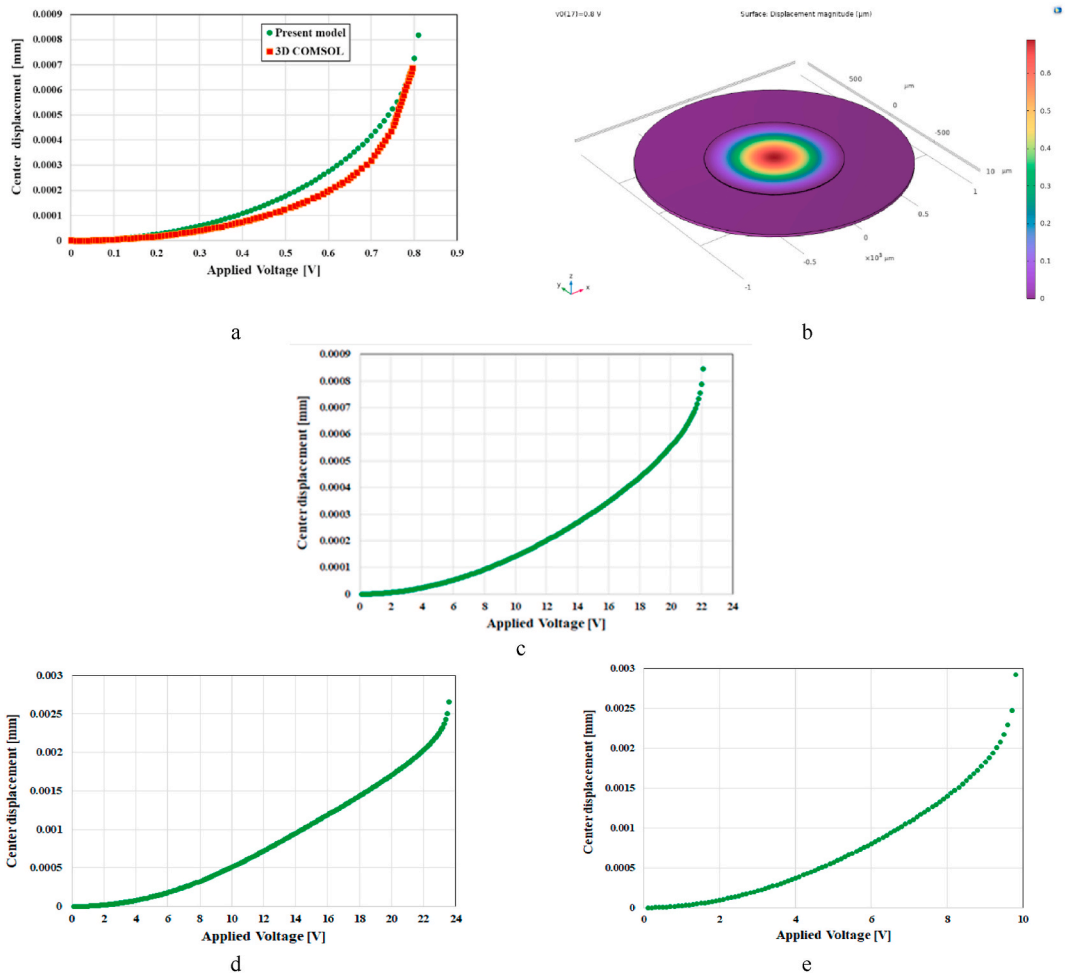

Fig. 3. Pull-in voltage and center deflection: a (case 1 state 1), b (3D COMSOL), c (case 1 state 2), d (case 2 state 1), and e (case 2 state 2).

before pull-in is lesser. On the other hand, state 2 of case 1, due to increased stiffness by Porous Polymer Dielectric Material foundation force, can tolerate a much higher magnitude of pressure range for each bias voltage than the conventional case. Also, increasing the stiffness of the system caused a convex behavior for the curve of state 2 compared with the concave curves of state 1 of case 1. However, in case 2, completely inverse behavior has been seen. In Fig. 4c and d, the behavior of case 2 is shown. What is evident, the system shows contrary behavior. Using a softer polymer with different physical and geometrical configurations increased the sensitivity of the sensor and the measured pressure in the $\beta = 0.7$ of case 2 state 2 is lower than state 2 because of the higher sensitivity.

3.2. Dynamic analysis

To determine the dynamic transient solution of the system, a Hilbert-based expansion is employed to decompose the system over spatial coordinates. Integration over the time domain is then performed using direct integration techniques [48] Given that the problem involves nonlinearities stemming from various sources, such as nonlinear electrostatic force, displacement-dependent porosity, mid-plane stretching, and coupled nonlinearity arising from the nonlinear behavior of the foundation, a simplification is applied. All nonlinear terms are treated as known forcing terms at each integration step. These terms are continuously updated with the progression of time, facilitating the application of spatial coordinate decomposition and the solution of the problem.

In this method, for each applied DC voltage, time integration over the domain is applied to the differential equations to find the proper shape functions and the displacements. In the present part, the DC voltage is applied to the microplate of the Porous Polymer Dielectric Material case (case 1 state 2) as a coefficient of the statical pull-in voltage respectively for $\beta = 0.3$, $\beta = 0.5$, and, $\beta = 0.7$. The time step of the integration (Solution of the Runge-Kutta method) is $\Delta t = 10^{-8}$ s and it is chosen for more accurate results and convergency. Also, the pressure is applied in different conditions such as constant pressure during the solution, as a step function and applied in the 100 times steps in the different scenarios at the beginning of the solution and the middle of the solution, and impulse function which is applied just for one-time step during the dynamic analysis for each case. Henceforth the results are compared to each other. Fig. 5, indicates the dynamic response of the case with the Porous Polymer Dielectric Material for the pressure as the step

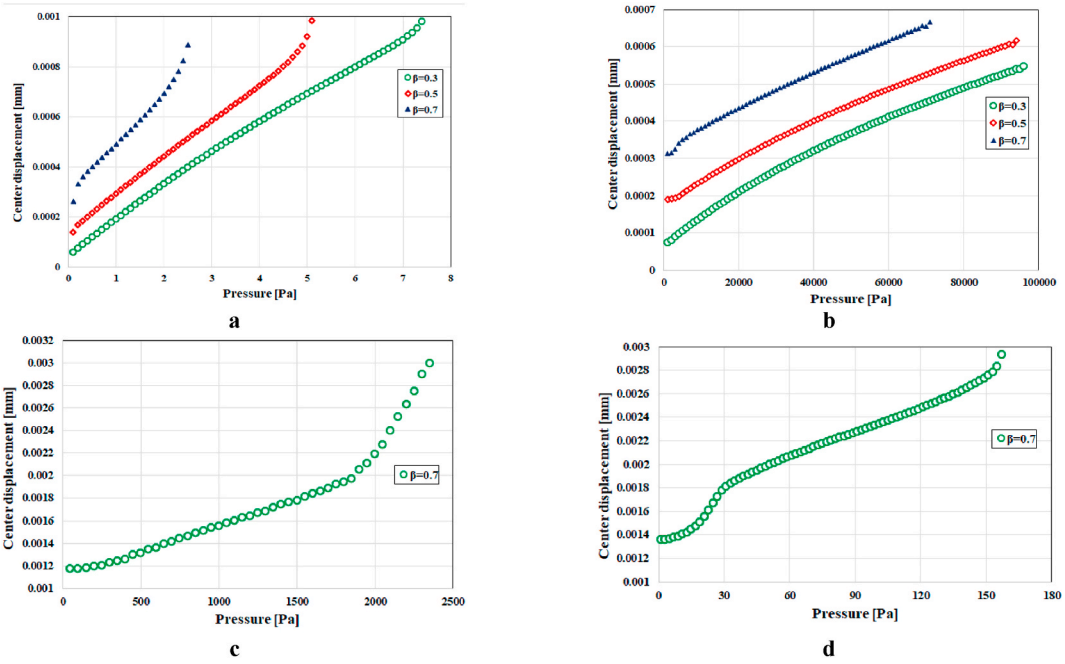

Fig. 4. Center displacement while applying a constant pressure: a (case 1 state 1) and b (case 1 state 2).

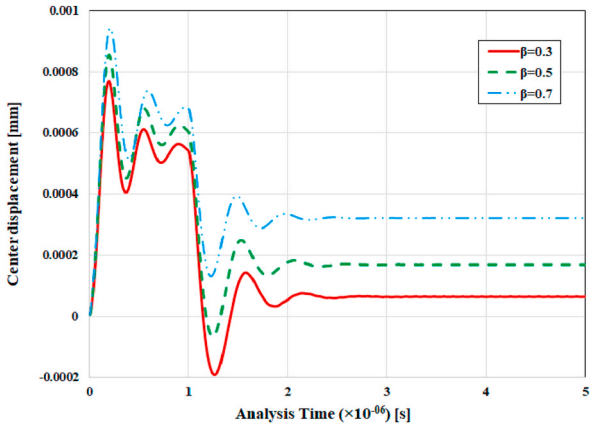

Fig. 5. Dynamic response of case 1 state 2 for the pressure applied as a step function.

function. The pressure is constantly applied for the 100 times steps at the beginning of the solution for different DC voltage coefficients. As it is clear, after the pressure is removed, the three states have the same response and trend due to the same physical and geometrical configuration. However, by augmentation of the voltage coefficient, the maximum center displacement is also enhanced because of the increasing force that is applied to the microplate.

Fig. 6 shows the dynamic response of the different bias voltage coefficients for the applied pressure as the step function at the middle of the solution. As it is visible, the pressure is applied from 300 times steps to 400 times steps and the responses are compared to each other. It is clear that the time responses are the same and the center displacement is also in this case same as Fig. 5. The maximum bias voltage has the maximum center displacement.

In Fig. 7, the dynamic response of the cases for the pressure is applied as an impulse function at the beginning of the solution is indicated. Impulsive pressure has a great impact on the dynamic response. In this case, the trend of the curves is the same, however, the case with $\beta = 0.7$ has the maximum displacement. The reason is the augmentation of the DC voltage, empowers the excitation force which leads to a great displacement. Also, since the pressure acts in a short time, it does not have a big effect on the response compared with the bias voltage.

Fig. 8 shows the dynamic response for the constant pressure which acts during the solution along with the bias voltage. In this state, the pressure has a great impact on the response of the microplate, because it acts constantly in all time steps of the solution. As can be

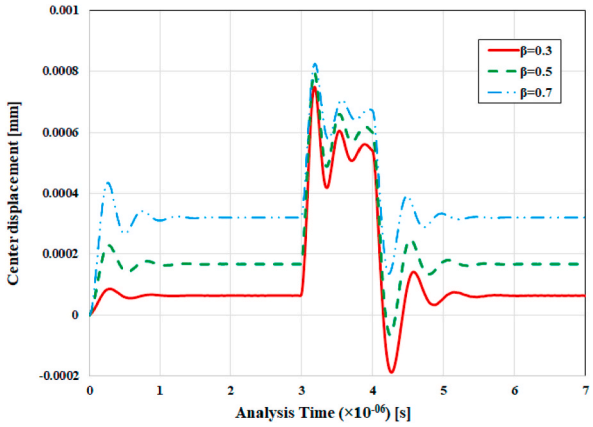

Fig. 6. Dynamic response of case 1 state 2 for the pressure applied as a step function.

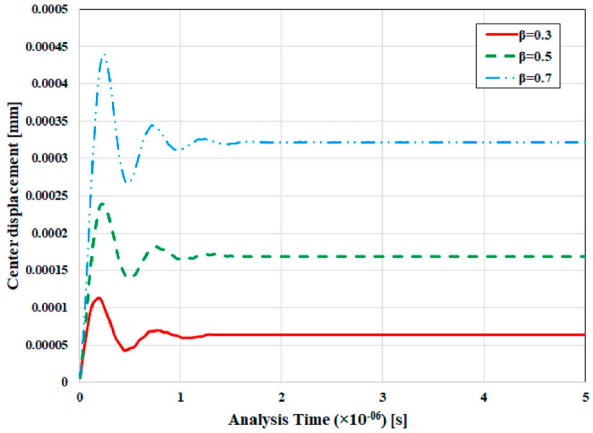

Fig. 7. Dynamic response of case 1 state 2 for the pressure applied as an impulse function.

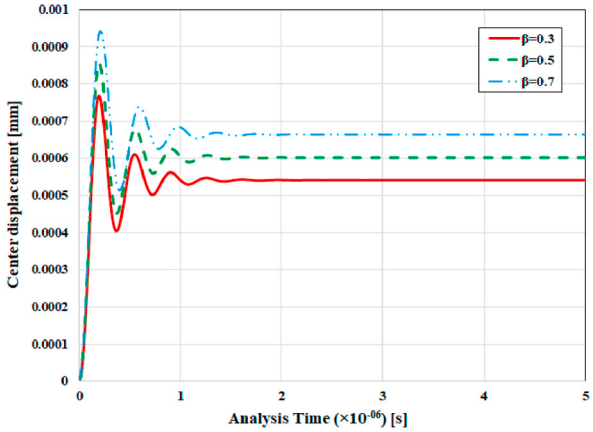

Fig. 8. Dynamic response of case 1 state 2 for the pressure applied as a constant value during the dynamic solution.

seen in the Figure, the $\beta = 0.7$ shows a slight increase in the center displacement due to a big value of the bias voltage. The small differences between the responses are due to the greater values of the pressure for cases with small bias voltages. It should be noted that the value of the acting pressure for each bias voltage is extracted from Fig. 4b, which is 96 kPa, 92 kPa, and 73 kPa for $\beta = 0.3$ to 0.7 respectively.

3.3. Frequency response analysis

The Frequency Response (F.R) is performed in the cases with and without Porous Polymer Dielectric Material in the gap for the small and big values of the excitation voltages and pressures respectively. Fig. 9 (a and b) show the Frequency Response for the case without and with Porous Polymer Dielectric Material respectively.

In Fig. 9, it is obvious that the resonance occurs when the excitation frequency approaches the natural frequency of the system. In this part, the alternative voltages are the same for all cases, although, the V_{DC} is varied for different bias voltages. By increasing the V_{DC}, as expected, the resonance frequency of the system decreases for all cases because of the softening of the system by increasing the excitation force. The main result is that the effect of changing the V_{DC} is more significant in the case of Porous Polymer Dielectric Material than the conventional one. Also, the natural frequency of the system for the case with Porous Polymer Dielectric Material is increased about 100 times due to hardening the system. In the present part, the applied pressure is assumed to be zero. Fig. 10 (a and b) indicate the Frequency Response of the case without and with Porous Polymer Dielectric Material respectively for changing the alternative voltage (V_{AC}). In this part, the V_{DC} is the same for all cases and the coefficient is $\beta = 0.3$.

In Fig. 10, it is seen that increasing the V_{AC} does not affect the resonance frequency and it just increases the center displacement altitude. Fig. 11 (a and b) demonstrates the Frequency Response of the cases without and with Porous Polymer Dielectric Material for changing the P_{Al} (alternative part of the applied pressure). In this part, the P_0 (Constant part of the applied pressure) is 3 Pa and 50 kPa for the cases without and with Porous Polymer Dielectric Material respectively, and just the alternative term of equation 46 is varied while the coefficient of the bias voltage is kept in $\beta = 0.3$.

Exciting pressure increasing just can raise the amplitude of the displacement of the microplate and it does not affect the resonance frequency for both cases which is shown clearly in Fig. 11.

All of the results which have obtained above are for the small magnitudes of the excitation forces. Therefore, as can be seen from the Frequency Response, the responses are linear and have not seen any nonlinearity in the responses. In the following, the magnitudes of the excitation forces are enhanced to raise the nonlinearity of the equations, and the results are indicated below. Fig. 12 indicates the Frequency Response of the changing the bias voltage coefficient while the $V_{AC} = 0.3V$. Growing the bias DC voltage softens the system and the resonance frequency is decreased. Afterward, when the DC voltage is augmented about $\beta = 0.8$ the nonlinear behavior of the response is revealed. When the DC voltage coefficient is increased, the exerted force can dominate the system stiffness and the nonlinear softening of the system is obvious.

In Fig. 13 the behavior of the response of the case without Porous Polymer Dielectric Material is studied for different V_{AC} while the coefficient of the DC voltage is kept at $\beta = 0.8$. The results demonstrate that increasing the alternative voltages about $V_{AC} = 0.3V$ caused the nonlinear behavior in the response because of the system softening.

Fig. 14 illustrates the Frequency Response of the case without Porous Polymer Dielectric Material for changing the alternative term of the pressure. In this part, the constant term of the pressure is assumed 1.4 Pa, $\beta = 0.7$, and the alternative pressure (P_{Al}) is changed.

Raising the P_{Al} in this case can lessen the system stiffness, thus, the resonance frequency tends to the left-hand side.

Fig. 15 displays the response of the case with Porous Polymer Dielectric Material for different V_{AC}. In this case, the bias voltage coefficient is $\beta = 0.7$, no pressure is applied and just the alternative voltage is changed.

In high values of V_{AC}, the case with Porous Polymer Dielectric Material displays a special behavior. As displayed in Fig. 15, raising the V_{AC} in the case of Porous Polymer Dielectric Material leads to system hardening in a nonlinear manner.

The nonlinear behavior of the case of Porous Polymer Dielectric Material is indicated in Fig. 16. In this case, the Constant pressure term is fixed at 50 kPa, $\beta = 0.7$, and P_{Al} is raised from 1 kPa to 20 kPa. As is indicated, higher magnitudes of the alternative pressure term cause system hardening. Raising the P_{Al} leads to higher magnitudes of the system stiffness and in this case, the Porous Polymer Dielectric Material caused to increase the nonlinearity of the system.

Fig. 17 displays the Frequency Response of case 2 state 2 for various V_{AC}. Increasing the VAC does not change the system resonance while causing system hardening and nonlinear behavior.

In Fig. 18 the Frequency Response of case 2 states 2 versus the changing the P_{Al} is shown. In the lower alternative pressure, the system's behavior remains linear and the system tends to soften. Nevertheless, increasing the P_{Al} leads to system hardening and increasing the nonlinearity of the system, while the resonance frequency is kept fixed.

In this paper, the impact of the changing porosity of the Porous Polymer Dielectric Material on the Frequency Response of the system is also considered. For this purpose, the porosity of the dielectric is increased from 0.1 to 0.2 and the Frequency Response of the system is demonstrated in Fig. 19 for different V_{ac}. It should be noted that the geometrical configuration of this case is the same as the case 1 state 2 and just porosity is changed to 0.2. The change in the porosity just shifts the resonance frequency a little to lower values due to decreasing the foundation force of the dielectric, compared with Fig. 15. However, the trend and the sample of curves remain constant.

4. Conclusion

In the present work, a novel design of a capacitive pressure sensor is introduced that uses a Porous Polymer Dielectric Material as a dielectric in the gap between the fixed and flexible circular microplates. Mathematical governing equations of the problem were extracted for both the flexible microplate and Porous Polymer Dielectric Material squeeze motion. The equations are discretized numerically using the Galerkin weighted residual model. For the static modeling, the time-dependent parts derivatives are assumed zero and then algebraic equations are solved to obtain the displacement of the microplate. For the dynamic transient analysis, the ordinary differential equations gained by the Galerkin method are solved using the 4th-order Runge-Kuta method and for the steady

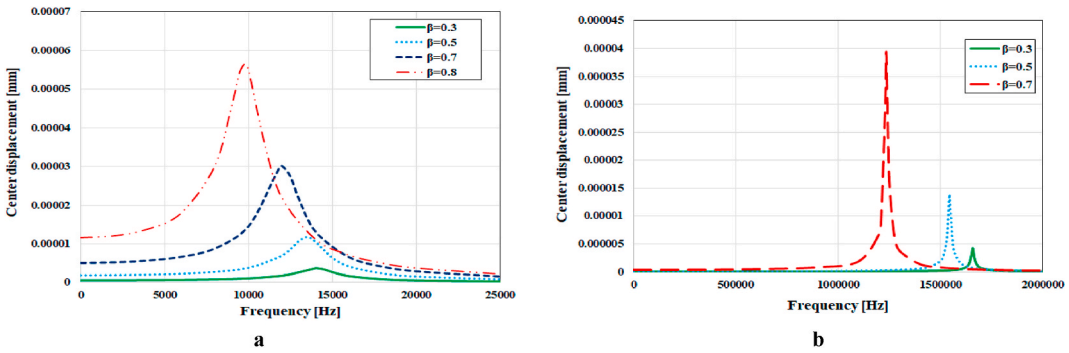

Fig. 9. Frequency Response for the $V_{AC} = 0.01V$. a (case 1 state 1) and b (case 1 state 2).

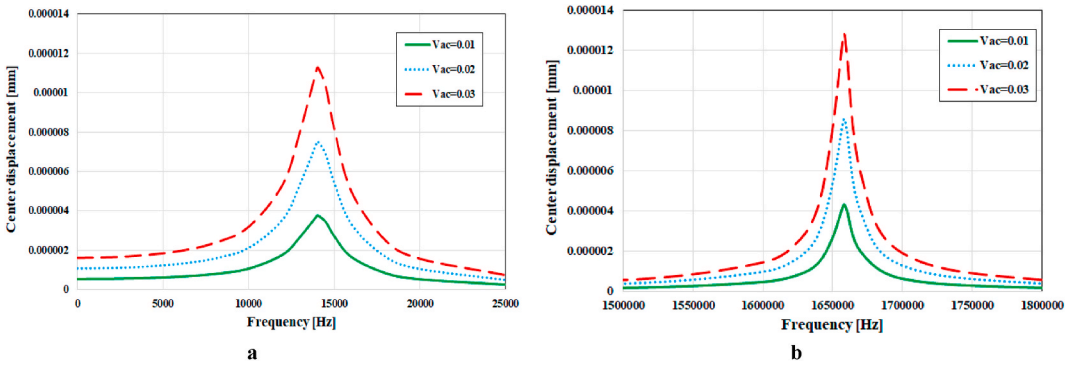

Fig. 10. Frequency Response for the $V_{AC} = 0.01V$. a (case 1 state 1) and b (case 1 state 2).

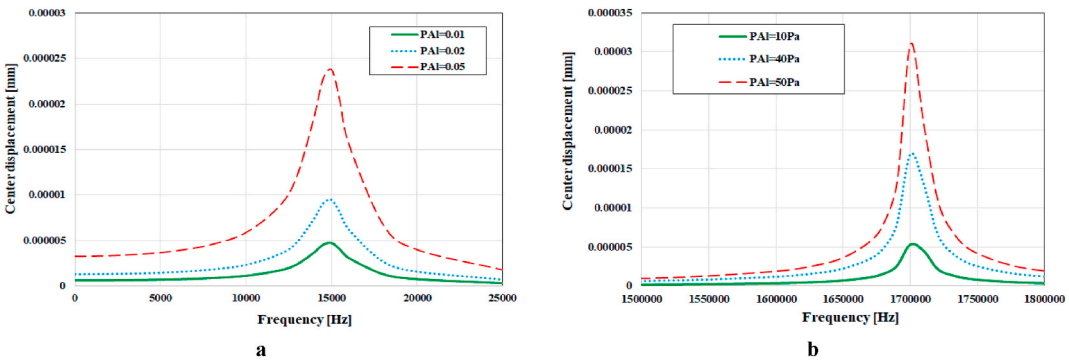

Fig. 11. Frequency Response for the applied pressure. a (case 1 state 1) and b (case 1 state 2).

state solution, the coefficients of the presented periodic solution are obtained by finding the roots of the energy balance equation by a learning approach through physically gradient-decent based method. At first, the results of the case without Porous Polymer Dielectric Material are compared to the numerical and experimental data which has a very good agreement. Afterward, the following results are obtained.

- The results of the static analysis revealed that case 1 state 2 augmented the system stiffness and so the pull-in voltage is increased compared to state 1, from 0.81V to 22V.
- The bias voltages for all cases and states (with and without Porous Polymer Dielectric Material) along with the constant pressure which is applied to the flexible plate as the external force, are calculated and it is seen that case 1 state 2 can sustain a much more magnitude of the pressure comparing with the state 1 case. In this state, the voltage is applied as the coefficients of the pull-in voltage for each case. But, in case 2, it is completely inverted, so state 2 of case 2 is more sensitive than state 1.
- The dynamic analysis is performed for the case with Porous Polymer Dielectric Material. In this part, the external forces are the bias voltage for the different coefficients ($\beta = 0.3$, $\beta = 0.5$, and $\beta = 0.7$) along with the pressure which is inducted as the constant value,

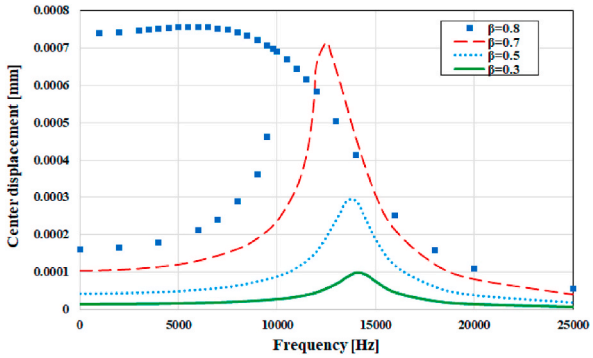

Fig. 12. Frequency Response for the different V_{DC} for case 1 state 2.

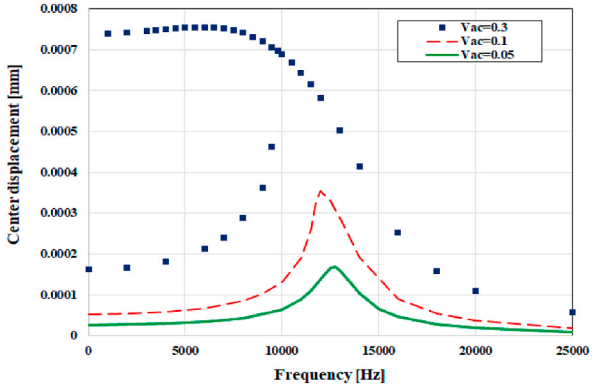

Fig. 13. Frequency Response for the different V_{AC} for case 1 state 1.

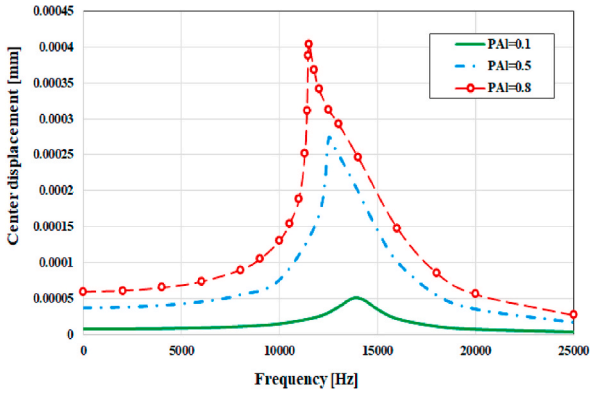

Fig. 14. Frequency Response for the different P_{Al} for case 1 state 1.

step function in some time steps, and as an impulsive pressure for a time step. After applying the pressure, it is indicated in the Figures that the system acylates and finally, it approaches the static response magnitudes.

- In both cases, the increase of the V_{DC} leads to the system softening and decreases the resonance frequency. However, the existence of the Porous Polymer Dielectric Material will cause an increase in the stiffness of the system which increases the natural frequency by about 100 and 10 times bigger in cases 1 and 2 respectively.
- The Frequency Response analysis is composed of two parts one for the small alternative forces (V_{AC} and P_{Al}) which keep the system behavior linear and the second one for the big values of the alternative forces which lead to the nonlinear behavior of the system.
- The results demonstrate that increasing the V_{AC} and P_{Al} in state 1 causes to the system soften, however, in case 2, it causes to the system harden because of the nonlinear behavior of the Porous Polymer Dielectric Material.

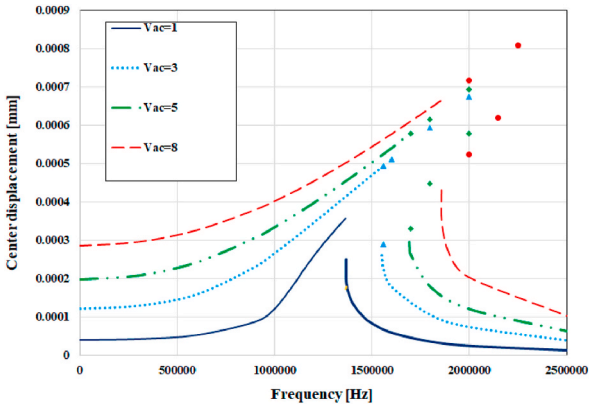

Fig. 15. Frequency Response for the different V_{AC} for case 1 state 2.

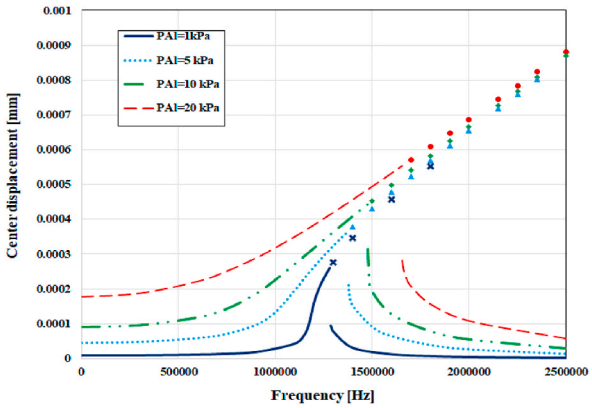

Fig. 16. Frequency Response for the different P_{AI} for case 1 state 2.

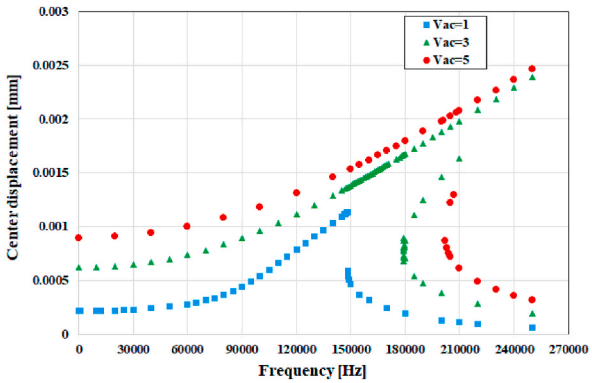

Fig. 17. Frequency Response for the different V_{AC} for case 1 state 2.

- Increasing the sensitivity of the capacitive device or the pressure sensor by using the Porous Polymer Dielectric depends on the geometrical configuration and the physical properties of both plates and the polymer. As a result, in some cases using the polymer as a dielectric can increase the sensitivity while it can act in reverse.
- Therefore, engineers and researchers should be cautious in using polymer materials as dielectric fillers in MEMS capacitive devices and as a future work plan, it is crucial to deeply study the geometric and material properties as well as the effect of porosity of porous polymer dielectric materials on the static, dynamic and frequency response of the sensor through different stress-stretch constitutive models, which consequently will lead to generalizing of the findings.

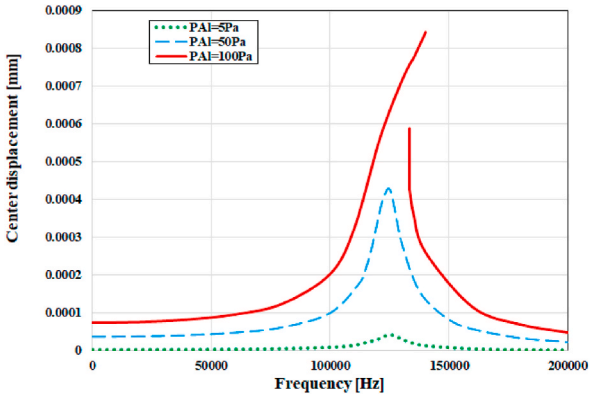

Fig. 18. Frequency Response for the different P_{AI} for case 2 state 2.

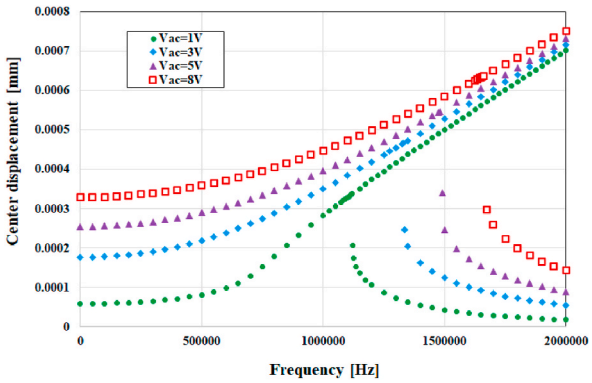

Fig. 19. Frequency Response for the different V_{AC} for $\forall_p^{(0)} = 0.2$.

Data availability

Data sharing does not apply to this article as no datasets were generated or analyzed during the current study.

CRediT authorship contribution statement

Nima Ahmadi: Writing – original draft, Validation, Software. **Ghader Rezazadeh:** Writing – review & editing, Supervision, Investigation, Funding acquisition, Conceptualization. **Arash Rahmani:** Writing – review & editing, Writing – original draft, Software. **Mina Ghanbari:** Writing – review & editing, Writing – original draft, Validation, Software.

Declaration of competing interest

The authors whose names are listed immediately below certify that they have NO conflict of interest.

Acknowledgment

This work was financially supported by the Ministry of Science and Higher Education of the Russian Federation (Project No. FENU 2023-0010).

References

[1] Waleed Faris, Ali H. Nayfeh, Mechanical response of a capacitive microsensor under thermal load, Commun. Nonlinear Sci. Numer. Simulat. 12 (5) (2007) 776–783.
[2] Behrokh Abbasnejad, Ghader Rezazadeh, Mechanical behavior of a FGM micro-beam subjected to a nonlinear electrostatic pressure, Int. J. Mech. Mater. Des. 8 (2012) 381–392.
[3] L. Yu, B.J. Kim, E. Meng, Chronically implanted pressure sensors: challenges and state of the field, Sensors 14 (11) (2014) 20620–20644.
[4] Pierpaolo Belardinelli, Banafsheh Sajadi, Stefano Lenci, Farbod Alijani, Global dynamics and integrity of a micro-plate pressure sensor, Commun. Nonlinear Sci. Numer. Simulat. 69 (2019) 432–444.

[5] S. Li, Y. Gu, G. Wu, K. Dong, M. Jia, D. Zhang, X. Xiao, A flexible piezoresistivesensor with highly elastic weave pattern for motion detection, Smart Mater. Struct. 28 (2019) 035020.
[6] Y. Gao, M. Xu, G. Yu, J. Tan, F. Xuan, Extrusion printing of carbonnanotube-coated elastomer fiber withmicrostructures for flexible pressuresensors, Sens. Actuator. A-Phys. 299 (2019) 111625.
[7] S. Chen, Z. Lou, D. Chen, Z. Chen, K. Jiang, G. Shen, Highly flexible strain sensorbased on ZnO nanowires and P(VDF-TrFE) fibers for wearable electronicdevice, Sci. China Mater. 59 (2016) 173–181.
[8] Guanzheng Wu, Siming Li, Jiayu Hu, Manchen Dong, Ke Dong, Xiuliang Hou, Xueliang Xiao, A capacitive sensor using resin thermoplastic elastomer and carbon fibers for monitoring pressure distribution, Pigment Resin Technol. 50 (5) (2020) 437–443.
[9] S. Li, T. Chen, X. Xiao, Periodically inlaid carbon fiber bundles in the surface ofhoneycomb woven fabric for fabrication of normal pressure sensor, J. Mater. Res. 55 (2020) 6551–6565.
[10] Young Jung, Wookjin Lee, Kyungkuk Jung, Byunggeon Park, Jinhyoung Park, Jongsoo Ko, Hanchul Cho, A highly sensitive and flexible capacitive pressure sensor based on a porous three-dimensional PDMS/microsphere composite, Polymers 12 (6) (2020) 1412.
[11] Qian Zhou, Bing Ji, Yuzhang Wei, Bin Hu, Yibo Gao, Qingsong Xu, Jun Zhou, Bingpu Zhou, A bio-inspired cilia array as the dielectric layer for flexible capacitive pressure sensors with high sensitivity and a broad detection range, J. Mater. Chem. A 7 (48) (2019) 27334–27346.
[12] Jiahui Guo, Yunru Yu, Dagan Zhang, Han Zhang, Yuanjin Zhao, Morphological Hydrogel Microfibers with MXene Encapsulation for Electronic Skin, 2021. Research 2021.
[13] Otto Wichterle, Drahoslav Lim, Hydrophilic gels for biological use, Nature 185 (4706) (1960) 117–118.
[14] P.H. Corkhill, C.J. Hamilton, B.J. Tighe, Synthetic hydrogels VI. Hydrogel composites as wound dressings and implant materials, Biomaterials 10 (1989) 3–10.
[15] Lisa Brannon-Peppas, Nikolaos A. Peppas, Time-dependent response of ionic polymer networks to pH and ionic strength changes, Int. J. Pharm. 70 (1–2) (1991) 53–57.
[16] Darren J. Lipomi, Michael Vosgueritchian, CK Tee Benjamin, Sondra L. Hellstrom, Jennifer A. Lee, Courtney H. Fox, Bao Zhenan, Skin-like pressure and strain sensors based on transparent elastic films of carbon nanotubes, Nat. Nanotechnol. 6 (12) (2011) 788–792.
[17] Baoqing Nie, Ruya Li, Jennifer Cao, James D. Brandt, Tingrui Pan, Flexible transparent iontronic film for interfacial capacitive pressure sensing, Adv. Mater. 27 (39) (2015) 6055–6062.
[18] Xiandi Wang, Dong Lin, Hanlu Zhang, Ruomeng Yu, Caofeng Pan, Lin Wang Zhong, Recent progress in electronic skin, Adv. Sci. 2 (10) (2015) 1500169.
[19] Kalpana R. Kamath, Park Kinam, Biodegradable hydrogels in drug delivery, Adv. Drug Deliv. Rev. 11 (1–2) (1993) 59–84.
[20] W.E. Hennink, CF van Nostrum. "Advanced drug deliveries review.", Dep. Pharm. Utr. Univ 54 (2002) 13–36.
[21] E.H. Schacht, Polymer chemistry and hydrogel systems, J Phys: Conf Ser 3 (2004) 22.
[22] Stefan CB. Mannsfeld, Benjamin CK. Tee, Randall M. Stoltenberg, Christopher V. Chen, Soumendra Barman, Beinn VO. Muir, Anatoliy N. Sokolov, Colin Reese, Zhenan Bao, Highly sensitive flexible pressure sensors with microstructured rubber dielectric layers, Nat. Mater. 9 (10) (2010) 859–864.
[23] Sujie Chen, Bengang Zhuo, Xiaojun Guo, Large area one-step facile processing of microstructured elastomeric dielectric film for high sensitivity and durable sensing over wide pressure range, ACS Appl. Mater. Interfaces 8 (31) (2016) 20364–20370.
[24] Mina Ghanbari, Ghader Rezazadeh, Vahid Moloudpour-Tolkani, Nonlinear dynamics of a tunable novel accelerometer, tunable with a microtriple electrode variable capacitor, Acta Mech. (2023) 1–22.
[25] Mina Ghanbari, Ghader Rezazadeh, Vahid Moloudpour-Tolkani, A wide-bandwidth MEMS energy harvester based on a novel voltage-sliding stiffness tunability, Appl. Math. Model. 125 (2024) 16–34.
[26] Seolhee Baek, Hayeong Jang, So Young Kim, Heejeong Jeong, Singu Han, Yunseok Jang, Do Hwan Kim, Hwa Sung Lee, Flexible piezocapacitive sensors based on wrinkled microstructures: toward low-cost fabrication of pressure sensors over large areas, RSC Adv. 7 (63) (2017) 39420–39426.
[27] Benjamin C-K. Tee, Alex Chortos, Roger R. Dunn, Gregory Schwartz, Eric Eason, Zhenan Bao, Tunable flexible pressure sensors using microstructured elastomer geometries for intuitive electronics, Adv. Funct. Mater. 24 (34) (2014) 5427–5434.
[28] Tie Li, Hui Luo, Qin Lin, Xuewen Wang, Zuoping Xiong, Haiyan Ding, Yang Gu, Zheng Liu, Ting Zhang, Flexible capacitive tactile sensor based on micropatterned dielectric layer, Small 12 (36) (2016) 5042–5048.
[29] Shasha Duan, Ke Yang, Zhihui Wang, Mengting Chen, Ling Zhang, Hongbo Zhang, Chunzhong Li, Fabrication of highly stretchable conductors based on 3D printed porous poly (dimethylsiloxane) and conductive carbon nanotubes/graphene network, ACS Appl. Mater. Interfaces 8 (3) (2016) 2187–2192.
[30] Qi Li, Tiantian Duan, Jian Shao, Hongbin Yu, Fabrication method for structured porous polydimethylsiloxane (PDMS), J. Mater. Sci. 53 (16) (2018) 11873–11882.
[31] Shuying Wu, Jin Zhang, Raj B. Ladani, Anil R. Ravindran, Adrian P. Mouritz, Anthony J. Kinloch, Chun H. Wang, Novel electrically conductive porous PDMS/carbon nanofiber composites for deformable strain sensors and conductors, ACS Appl. Mater. Interfaces 9 (16) (2017) 14207–14215.
[32] Yeongjun Kim, Shin Jang, Je Hoon Oh, Fabrication of highly sensitive capacitive pressure sensors with porous PDMS dielectric layer via microwave treatment, Microelectron. Eng. 215 (2019) 111002.
[33] Siming Li, Ke Dong, Ruiqing Li, Xiayan Huang, Tianjiao Chen, Xueliang Xiao, Capacitive pressure sensor inlaid a porous dielectric layer of superelastic polydimethylsiloxane in conductive fabrics for detection of human motions, Sensor Actuator Phys. 312 (2020) 112106.
[34] MyongChol Kang, Ri Chan, JongHuan Choe, Capacitance response of concave well substrate touch-mode capacitive pressure sensor: mathematical analysis and simulation, Microelectron. J. 114 (2021) 105118.
[35] Ruiqing Li, Qun Zhou, Yin Bi, Shaojie Cao, Xue Xia, Aolin Yang, Siming Li, Xueliang Xiao, Research progress of flexible capacitive pressure sensor for sensitivity enhancement approaches, Sensor Actuator Phys. 321 (2021) 112425.
[36] Xingwei Tang, Qiao Gu, Ping Gao, Weijia Wen, Ultra-sensitive wide-range small capacitive pressure sensor based on porous CCTO-PDMS membrane, Sensors and Actuators Reports 3 (2021) 100027.
[37] Zhuyu Ma, Kaiyi Zhang, Shengdu Yang, Yang Zhang, Xianchun Chen, Qiang Fu, Hua Deng, High-performance capacitive pressure sensors Fabricated by introducing dielectric filler and conductive filler into a porous dielectric layer through a Biomimic strategy, Compos. Sci. Technol. 227 (2022) 109595.
[38] Yan Zhong, Fucheng Gu, Longgang Wu, Jiaqi Wang, Shengping Dai, Hao Zhu, Guanggui Cheng, Jianning Ding, Porous conductive electrode for highly sensitive flexible capacitive pressure sensor over a wide range, J. Alloys Compd. 934 (2023) 167919.
[39] Yunong Zhao, Xiaohui Guo, Weiqiang Hong, Tong Zhu, Tianxu Zhang, Zihao Yan, Kangli Zhu, et al., Biologically imitated capacitive flexible sensor with ultrahigh sensitivity and ultralow detection limit based on frog leg structure composites via 3D printing, Compos. Sci. Technol. 231 (2023) 109837.
[40] Eshwar Thouti, Kanika Chauhan, Rahul Prajesh, Mohd Farman, Ranjan Kumar Maurya, Prashant Sharma, Atmakuru Nagaraju, Flexible capacitive pressure sensors using microdome like structured polydimethylsiloxane dielectric layers, Sensor Actuator Phys. 335 (2022) 113393.
[41] Samia Achouch, Rihab Bousseta, Fakhita Regragui, Mourad Gharbi, Conception and realization of a novel design for a capacitive pressure sensor with high sensitivity and linear response, Results in Engineering 15 (2022) 100535.
[42] Takahiro Namazu, Yoshitada Isono, Takeshi Tanaka, Evaluation of size effect on mechanical properties of single crystal silicon by nanoscale bending test using AFM, J. Microelectromech. Syst. 9 (4) (2000) 450–459.
[43] Ali R. Hadjesfandiari, Edward P. Furlani, Arezoo Hajesfandiari, Gary F. Dargush, Size effects in vibrating silicon crystal microbeams, J. Eng. Mech. 145 (2) (2019) 04018136.
[44] Teddy Fen-Chong, Antonin Fabbri, Jean-Pierre Guilbaud, Olivier Coussy, Determination of liquid water content and dielectric constant in porous media by the capacitive method, Compt. Rendus Mec. 332 (8) (2004) 639–645.
[45] Xing-Da Liu, Zhi-Ling Hou, Bao-Xun Zhang, Ke-Tao Zhan, Peng He, Kai-Lun Zhang, Wei-Li Song, A general model of dielectric constant for porous materials, Appl. Phys. Lett. 108 (10) (2016).
[46] Lei Shi, Ruisen Yang, Shiyao Lu, Kun Jia, Chunhui Xiao, Tongqing Lu, Tiejun Wang, Wei Wei, Hui Tan, Shujiang Ding, Dielectric gels with ultra-high dielectric constant, low elastic modulus, and excellent transparency, NPG Asia Mater. 10 (8) (2018) 821–826.

[47] Shixue Wang, Yulin Wang, Investigation of the through-plane effective oxygen diffusivity in the porous media of PEM fuel cells: effects of the pore size distribution and water saturation distribution, Int. J. Heat Mass Tran. 98 (2016) 541–549.
[48] Enis Tuncer, The Landau-Lifshitz/Looyenga Dielectric Mixture Expression and its Self-Similar Fractal Nature, 2005 arXiv preprint cond-mat/0503750.
[49] Qinghua Lei, John-Paul Latham, Jiansheng Xiang, Chin-Fu Tsang, Philipp Lang, Liwei Guo, Effects of geomechanical changes on the validity of a discrete fracture network representation of a realistic two-dimensional fractured rock, Int. J. Rock Mech. Min. Sci. 70 (2014) 507–523.
[50] Aghababaie Beni, Mohamad-Reza Ghazavi Mahdi, Ghader Rezazadeh, A study of fluid media and size effect on dynamic response of microplate, Modares Mechanical Engineering 17 (9) (2017) 153–164.
[51] Xing-Da Liu, Zhi-Ling Hou, Bao-Xun Zhang, Ke-Tao Zhan, Peng He, Kai-Lun Zhang, Wei-Li Song, A general model of dielectric constant for porous materials, Appl. Phys. Lett. 108 (10) (2016).
[52] A.H. Nayfeh, P.F. Pai, Linear and Nonlinear Structural Mechanics, John Wiley & Sons, 2008.
[53] Adel Nabian, Ghader Rezazadeh, Mohammadali Haddad-Derafshi, Ahmadali Tahmasebi, Mechanical behavior of a circular micro plate subjected to uniform hydrostatic and non-uniform electrostatic pressure, Microsyst. Technol. 14 (2008) 235–240.
[54] Zaher Rahimi, Ghader Rezazadeh, Mohammad Asadi, Nonlinear dynamic modeling of a micro-plate resonator considering damage accumulation, Acta Mech. 234 (7) (2023) 2933–2946.
[55] J. Kováčik, Correlation between elastic modulus, shear modulus, Poisson's ratio and porosity in porous materials, Adv. Eng. Mater. 10 (3) (2008) 250–252.
[56] Chang Long, Xinyu Xie, Jizhu Fu, Qiang Wang, Hongmei Guo, Wei Zeng, Wei Ning, Siliang Wang, Yi Xiong, Supercapacitive brophene-graphene aerogel as elastic-electrochemical dielectric layer for sensitive pressure sensors, J. Colloid Interface Sci. 601 (2021) 355–364.
[57] Amar Kapić, Andromachi Tsirou, Piero Giorgio Verdini, Sandro Carrara, Uncertainty analysis of polymer-based capacitive relative humidity sensor at negative temperatures and low humidity levels, Measurement 209 (2023) 112468.
[58] Hou-Chang Li, Meng-Yu Wang, Bin Liu, Juan Liu, Qi Wang, Xing-Dao He, Hau Ping Chan, Danling Wang, Jinhui Yuan, Qiang Wu, Temperature-independent relative humidity sensing properties of polymer micro-bottle resonators coated with graphene oxide, Measurement 196 (2022) 111199.
[59] Chen Huang, Zuguang Bian, Chengfeng Fang, Xiaoliang Zhou, Jizhou Song, Experimental and theoretical study on mechanical properties of porous PDMS, J. Appl. Mech. 85 (4) (2018) 041009.
[60] Zhengfeng Zhou, Xiaotao Yu, Linxin Yuan, Chuanqi Yan, Comparative study on the chemical and rheological properties of elastomer-based and resin-based HVMAs, Measurement 199 (2022) 111441.
[61] Varij Panwar, Gopinathan Anoop, Flexible piezoresistive strain sensor based on optimized elastomer-electronic polymer blend, Measurement 168 (2021) 108406.
[62] Hamed Sadeghian, Ghader Rezazadeh, Comparison of generalized differential quadrature and Galerkin methods for the analysis of micro-electro-mechanical coupled systems, Commun. Nonlinear Sci. Numer. Simulat. 14 (6) (2009) 2807–2816.
[63] O. Zarei, G. Rezazadeh, A novel approach to study of mechanical behavior of nem actuators using galerkin method, Int. J. Nanosyst. 1 (2) (2008) 161–169.
[64] A. Ern, J.L. Guermond, Theory and Practice of Finite Elements, vol. 159, Springer, New York, 2004, pp. xiv–524.
[65] Kaveh Rashvand, Ghader Rezazadeh, Hamed Mobki, Mergen H. Ghayesh, On the size-dependent behavior of a capacitive circular micro-plate considering the variable length-scale parameter, Int. J. Mech. Sci. 77 (2013) 333–342.
[66] P.M. Osterberg, Electrostatically Actuated Microelectromechanical Test Structures for Material Property Measurement, Doctoral dissertation, Massachusetts Institute of Technology, 1995.
[67] P. Raback, A. Pursula, Finite element simulation of the electromechanical pull-in phenomenon. European Congress on Computational Methods in Applied Sciences and Engineering ECCOMAS 2004, Jyvaskyla, 24-28 July 2004.
[68] Partha Pratim Sengupta, Pradip Kar, Basudam Adhikari, Influence of dielectric constant of polymerization medium on processability and ammonia gas sensing properties of polyaniline, Bull. Mater. Sci. 34 (2011) 261–270.
[69] Petr Humpolíček, Katarzyna Anna Radaszkiewicz, Zdenka Capáková, Jiří Pacherník, Patrycja Bober, Věra Kašpárková, Petra Rejmontová, Marián Lehocký, Petr Ponížil, Jaroslav Stejskal, Polyaniline cryogels: biocompatibility of novel conducting macroporous material, Sci. Rep. 8 (1) (2018) 135.